ELSEVIER

Journal of Power Sources 84 (1999) 175–182

JOURNAL OF POWER SOURCES

www.elsevier.com/locate/jpowsour

Correlation between CO surface coverage and selectivity/kinetics for the preferential CO oxidation over Pt/γ-Al_2O_3 and Au/α-Fe_2O_3: an in-situ DRIFTS study

M.M. Schubert *, M.J. Kahlich, H.A. Gasteiger [1], R.J. Behm

Abteilung Oberflächenchemie und Katalyse, Universität Ulm, D-89069 Ulm, Germany

Accepted 28 June 1999

Abstract

We present in-situ IR (DRIFTS) measurements on CO adsorption and preferential CO oxidation (PROX) in H_2-rich gas on Pt/γ-Al_2O_3 and Au/α-Fe_2O_3 catalysts at their envisaged operating temperatures of 200°C and 80°C, respectively, which in combination with kinetic data show that the underlying reason for the very different PROX reaction kinetics on these two catalysts is the difference in steady-state CO coverage. Whereas on the platinum catalyst this is always near saturation under reaction conditions, causing a negative reaction order (−0.4) and a p_{CO}-independent selectivity, the amount of adsorbed CO on the gold particles (indicated by an IR band at ~2110 cm^{-1}) strongly depends on the CO partial pressure. From the position of the IR band of CO adsorbed on Au/α-Fe_2O_3, the steady-state coverages on the Au surface are shown to be significantly below saturation, with an upper limit of approximately $\theta_{CO} = 0.2$. Low reactant surface concentrations on Au explain the positive reaction order with respect to p_{CO} (+0.55 at 80°C) as well as the observed decoupling of the CO and H_2 oxidation rates, which results in a loss of selectivity with decreasing p_{CO}.

Keywords: FTIR; PROX; Selective CO oxidation; H_2-rich gas; Platinum; Pt/Al_2O_3; Gold; Au/Fe_2O_3; Kinetics; Selectivity; CO adsorption; CO coverage; Carbon monoxide

1. Introduction

Highly dispersed Au supported on reducible oxides (e.g., Fe_2O_3, Co_3O_4, TiO_2) is a well-known catalyst for low temperature oxidation of carbon monoxide, which for example is being used for CO/O_2 recombination in CO_2-lasers [1]. Several groups examined different preparation methods, pretreatment procedures, and reaction kinetics on Au/metal oxide catalysts (see, e.g., Refs. [1–6]). Recently, these catalysts have gained attraction for the preferential oxidation of CO in H_2-rich gas (PROX), used for the purification of feed gas streams for polymer electrolyte membrane (PEM) fuel cells from a methanol reformer [7–9]. The mass-specific reaction rates [$mol_{CO}/(g_{Au} \cdot s)$] on supported Au catalysts are equally high at 80°C, and even lower temperatures, as compared to standard PROX catalysts such as Pt/γ-Al_2O_3 [10,11] and Ru/γ-Al_2O_3 [12] at their operating temperature [13] of 150°C–200°C. This, in principle, improves the cold-start properties in a fuel cell system and also allows for a thermal (and spatial) integration of the PROX unit with the PEM fuel cell stack in form of a thin second layer placed on top of the anode-side of the membrane electrode assembly (MEA) [14]. Since the efficiency, in particular with respect to the load-following behavior, of the PROX unit critically depends upon the rate of back-formation of CO from CO_2 via the reverse water gas shift reaction, a significantly improved performance can be expected at low temperatures, where the shift equilibrium becomes more favorable [15].

The general suitability of the Au catalysts for the PROX reaction was investigated in previous studies on a Au/α-Fe_2O_3 catalysts, where we determined the CO oxidation

* Corresponding author. E-mail: markus.schubert@chemie.uni-ulm.de

[1] Present address: Adam Opel, Global Alt. Propulsion Center, IPC 8190, D-65423 Rüsselsheim, Germany.

0378-7753/99/$ - see front matter
PII: S0378-7753(99)00314-6

rates and selectivity ($S = r^{CO}/(r^{CO} + r^{H_2})$, with r^{CO} and r^{H_2} being the oxidation rates of CO and H_2, respectively) in H_2-rich gas [9]. These studies revealed drastic differences in the reaction kinetics as compared to the PROX reaction over Pt/γ-Al_2O_3 which we had studied earlier [15–17]. While the selectivity of the Au/α-Fe_2O_3 catalyst decreased strongly with decreasing CO partial pressure (1.5–0.02 kPa) and increasing temperature (40°C–80°C), it remained constant on Pt/γ-Al_2O_3 for operating temperatures ≤ 200°C. It was proposed that these differences result from different steady state CO coverages on the two catalysts during the reaction, with the Pt catalyst operating at very high CO coverages, practically at saturation coverage, while the Au catalyst was expected to run at low CO coverages. Direct proof for these assumptions, which are crucial for the mechanistic understanding of the reactions, however, is still lacking. In the present article we will show and discuss results of a spectroscopic study using in-situ DRIFTS (diffuse reflectance FTIR), which clearly supports these ideas.

Following a brief description of the experimental setup and procedures, we will first discuss basic kinetic data on the PROX reaction on both catalysts. We then present in-situ DRIFTS measurements, during CO adsorption/selective oxidation at varying CO partial pressures, which yield direct information on the steady-state CO coverage under PROX operating conditions. These data show unambiguously that the steady state CO concentration is low on the gold particles compared to platinum. This difference is shown to lead to the observed independence of S vs. p_{CO} on Pt, while the selectivity on Au strongly decreases with decreasing p_{CO}. Finally, we show DRIFTS data on the temperature dependence of the CO coverage which support the above-conclusions and also rationalize the observed changes in the CO reaction order with temperature observed experimentally.

2. Experimental

The experiments were performed at a 3.15 wt.% Au/α-Fe_2O_3 catalyst (for preparation details, see Ref. [9]), which was conditioned at 400°C in a stream of 10% O_2/N_2 (20 Nml/min) for 30 min prior to reaction (volumetric flow rates are expressed in terms of Nml/min, i.e., ml/min at standard conditions of $1.013 \cdot 10^5$ Pa and 273.15 K). The calcined catalyst has an average Au crystallite size of 6.5 nm (corresponding to a dispersion of ca. 24%), obtained from X-ray diffraction line-broadening of the Au(111) peak using the Scherrer equation.

For comparison a commercial 0.5 wt.% Pt/Al_2O_3 catalyst (Degussa F 213 XR/D) is used, which was conditioned at 350°C in 10% O_2N_2 (20 Nml/min, 30 min), followed by reduction in H_2 (20 Nml/min, 30 min). The dispersion of 38% (corresponding to an average particle diameter of around 4 nm) was determined by CO desorption (for more details, see Ref. [17]). The reactant gases H_2 (N5.0), N_2 (N6.0), 2% CO (N4.7) in H_2 (N5.6), 2% CO (N4.7) in N_2 (N6.0) and 10% O_2 (N5.0) in N_2 (N5.0; CO-free) were supplied by Linde, Messer Griesheim or MTI.

All reactions were carried out at atmospheric pressure. The DRIFTS measurements were performed in an in-situ reaction cell (modified Harricks model HV-DR2), which allowed continuous gas flow through the catalyst bed (ca. 0.1 g) during spectra acquisition. A *praying mantis* optical geometry (Harricks PM-DRA-2-XXX) was used to direct the infrared beam. The spectra were obtained on a Mattson Infinity AR 60 (resolution 4 cm^{-1}) and on a Nicolet Magna 560 (at 8 cm^{-1}) spectrometer, both equipped with a MCT narrow band detector, by coadding 300 single-beam spectra, equivalent to an acquisition time of ~ 2.5 min. All infrared data were evaluated in Kubelka–Munk units which are linearly related to the absorber concentration in DRIFTS. Spectral contributions from gas phase CO were eliminated by subtracting the corresponding spectra from the pure support material.

Kinetic measurements were conducted in a quartz tube (i.d. 4 mm) placed in a ceramic tube furnace (catalyst bed mass ca. 0.1 g) with on-line gas chromatograph analysis (DANI). A detailed description of the reactor and detection system has been reported elsewhere [17]. Experimental gas flow rates were between 100 and 135 Nml/min, corresponding to space velocities of $6–8 \cdot 10^4$ h^{-1}. To guarantee differential flow conditions, the catalysts were diluted with α-Al_2O_3. All rates are expressed as turnover frequencies TOFs, and the term *idealized reformate* refers to a mixture of up to 1.5% CO and variable amounts of O_2 in 75% H_2, balance N_2.

3. Results and discussion

3.1. Kinetic observations

Fig. 1 compares the turnover frequencies and selectivities of both catalysts at their envisaged operating temperatures during selective CO oxidation in idealized reformate at a constant λ-value of 2 ($\lambda = 2\,p_{O_2}/p_{CO}$), demonstrating the high activity of Au/α-Al_2O_3 at 80°C and its superior selectivity at high CO partial pressures. Assuming a simple power-law model for the CO oxidation kinetics, the slope in Fig. 1a corresponds to the sum of the reaction orders with respect to p_{O_2} and p_{CO} [17].

In microkinetic studies on the PROX over Pt/γ-Al_2O_3 at 150°C–250°C, the reaction orders with respect to p_{CO} and p_{O_2} were determined to be -0.4 and $+0.8$, respectively [17]. Mechanistically, this is consistent with the selective CO oxidation reaction occurring in the so-called *low-rate branch* [18]. In this reaction regime, the Pt sur-

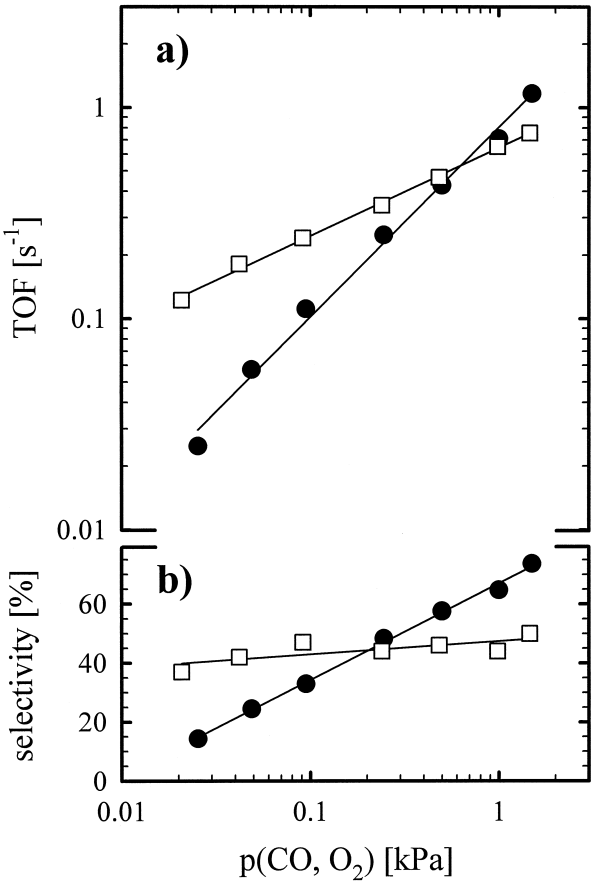

Fig. 1. Selective CO oxidation in idealized reformate at $\lambda = 2$ over $Pt/\gamma\text{-}Al_2O_3$ at 200°C (□) and $Au/\alpha\text{-}Fe_2O_3$ at 80°C (●): (a) CO oxidation rates; (b) selectivity.

face is thought to be completely covered by CO under reaction conditions, with dissociative O_2 adsorption being the rate limiting step [16]. Consequently, the oxidation rate of co-adsorbed hydrogen is also rate-limited by the same step (dissociative O_2 adsorption), so that CO and H_2 oxidation rates are coupled, effecting an essentially constant selectivity of ca. 40% (Fig. 1b) on $Pt/\gamma\text{-}Al_2O_3$ over the entire range of CO and O_2 partial pressures at temperatures below 250°C [17]. The following in-situ DRIFTS experiments were conducted to give further credence to the above-assumption of *low-rate branch* conditions during the PROX reaction on $Pt/\gamma\text{-}Al_2O_3$.

As already mentioned, the $Au/\alpha\text{-}Fe_2O_3$ catalyst shows a comparable activity at the much lower temperature of 80°C. However, from the different slope in Fig. 1a, it is already apparent that the reaction orders, i.e., the reaction kinetics, are very different on the gold catalyst. The reaction orders with respect to p_{CO} and p_{O_2} determined in microkinetic studies in idealized reformate were $+0.55$ and $+0.23$, respectively [9]. In terms of a mechanistic model, the positive CO reaction order suggests that there is no self-poisoning of the CO oxidation reaction by adsorbed CO, contrary to what is observed for the Pt catalyst. Boccuzzi et al. [19] proposed that the reaction follows a Langmuir–Hinshelwood type mechanism where both reactants are adsorbed on the Au surface, as it is well established for CO oxidation on platinum metal surfaces [18]. In this case, the positive CO reaction order implies that under reaction conditions, the CO coverage is significantly below saturation and hence a decrease of the CO partial pressure decreases the reaction probability for CO oxidation. The relatively high selectivity of the Au catalyst, particularly at high CO partial pressures (Fig. 1b), can be rationalized by the very low dissociative sticking probability for H_2 on a gold surface [20,21]. Assuming low CO coverages under PROX conditions, hydrogen dissociation would be expected to be essentially unperturbed by adsorbed CO, so that the H_2 oxidation rate (at constant p_{O_2}) should be independent from the CO oxidation rate which, indeed, is experimentally observed [9]. Consequently, a decrease in p_{CO} with a concomitant decrease in the CO oxidation rate results in the loss of selectivity shown in Fig. 1b, a striking difference to the behavior of the $Pt/\gamma\text{-}Al_2O_3$ catalyst. As mentioned above, the following in-situ DRIFTS experiments were conducted to support the suggested low CO coverage conditions during the PROX reaction on $Au/\alpha\text{-}Fe_2O_3$ [9,15,16].

3.2. Steady state CO coverage on $Pt/\gamma\text{-}Al_2O_3$

Since the DRIFTS signal depends on the penetration depth of the infrared beam into the powder catalyst sample and is a strong function of the support material, the particle size, and the packing density [22], a direct quantitative

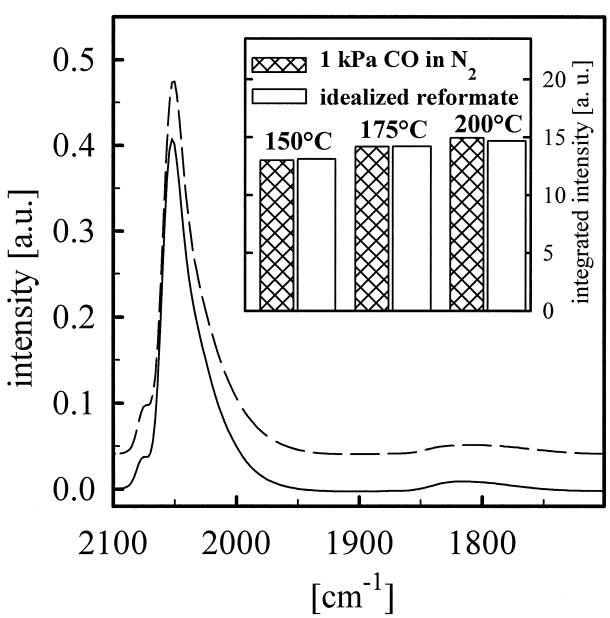

Fig. 2. DRIFTS spectra of the CO_{linear} band on $Pt/\gamma\text{-}Al_2O_3$ in 10 kPa CO in a pure N_2 background and during the selective CO oxidation in idealized reformate with 10 kPa CO and $\lambda = 2$ (dashed line). Inset: Comparison of the integrated IR intensities in a N_2 background (hatched bars) and under PROX conditions (unhatched bars) at different temperatures.

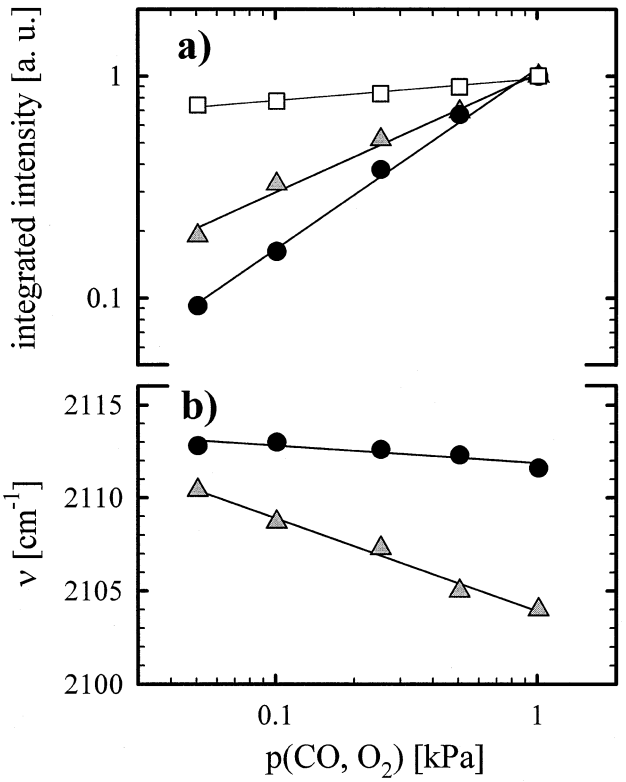

Fig. 3. IR intensity of linearly bonded CO during selective CO oxidation in idealized reformate at $\lambda = 2$ over Pt/γ-Al_2O_3 at 200°C (□) and Au/Fe_2O_3 at 80°C (●); IR intensity of linearly bonded CO on Au/α-Fe_2O_3 during CO adsorption in a pure N_2 background (△). (b) Corresponding band positions on Au/α-Fe_2O_3 during selective CO oxidation (●) and CO adsorption (△) at 80°C.

determination of the CO coverage from the DRIFTS spectra is generally not possible. Therefore, the experimental CO adsorption intensities measured during the PROX reaction by in-situ DRIFTS will be referenced to the CO_{ad} intensities produced by CO adsorption in a pure N_2 background. For the latter, the CO-coverage on Pt can be estimated using first order Langmuir adsorption–desorption kinetics for CO. Employing literature data for the CO adsorption energy at high coverages (e.g., 85 kJ/mol on Pt(111) [23], 97 kJ/mol on Pt(533) [24], and 151 kJ/mol on Pt(321) [25]), and standard values for the corresponding preexponential factors and the sticking coefficient of 10^{13} to 10^{16} s^{-1} and 0.5–0.8, respectively, we compute CO coverages which for a CO partial pressure of 10 kPa and temperatures up to 200°C in all cases are close to saturation ($\theta_{CO} > 0.9\theta_{sat}$).

DRIFTS spectra recorded under CO adsorption–desorption equilibrium (1 kPa CO, balance N_2) and during the PROX reaction (1 kPa CO, $\lambda = 2$, 75% H_2) are practically identical (see for 150°C in Fig. 2). In the inset to Fig. 2 we compare the integrated CO_{linear} band intensity of the two cases at different temperatures, which shows that the steady-state CO coverage is essentially unperturbed by the selective CO oxidation reaction. (The ratio between bridge and linear CO was constant in these experiments.) This is not surprising if we consider that under reaction conditions the kinetic equilibrium $r_{ad} = r_{des}$ has just to be expanded by the reaction process

$$r_{ad} = r_{des} + \text{TOF} \quad (1)$$

and that the additional term in Eq. (1), the CO turnover frequency, is on the order of 1 s^{-1} (see Fig. 1). This is more than two orders of magnitude lower than r_{des} if the above-quoted parameters for the CO adsorption kinetics are used. Therefore, essentially identical CO_{ad} intensities (see Fig. 2) are predicted on the basis of Eq. (1) (assuming that the IR cross-section of CO_{ad} is not significantly altered by the presence of O_2 and H_2). This, in conjunction with the above-estimated CO coverage based on the pure adsorption experiments provides strong evidence that the PROX reaction under the conditions of Fig. 2 does, indeed, occur at close to CO saturation coverage.

Based on Eq. (1) we can estimate that the CO coverage remains close to saturation during the reaction even at much lower CO partial pressures, reflecting the adsorption–desorption behavior in the high pressure regime of a Langmuir isotherm. This is confirmed by the DRIFTS measurements in Fig. 3a (square symbols), which show that the IR intensity and hence the steady-state CO coverage (see above) decreases by less than 20% as the CO partial pressure is reduced from 1 to 0.05 kPa. At the same time, the CO frequency remained almost constant at 2050 cm^{-1} (not shown). Despite the slight loss in CO coverage, the adlayer is still sufficiently dense to efficiently inhibit the adsorption of H_2 (and O_2) during the reaction, explaining the small loss in selectivity (Fig. 1b, square symbols). Hence, over the entire pressure range in Fig. 1, selectivity

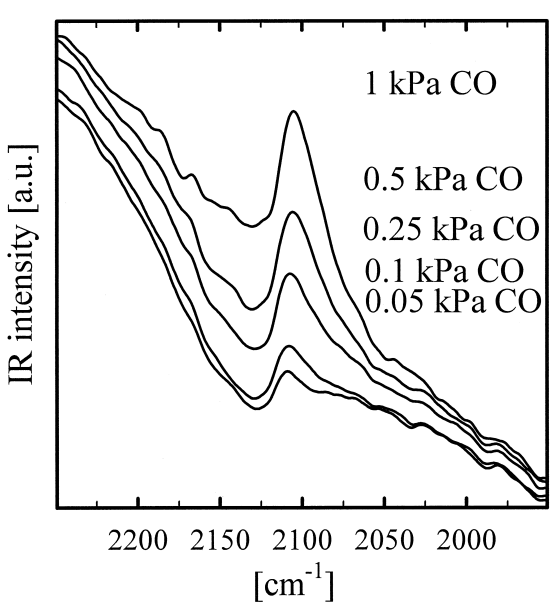

Fig. 4. In-situ DRIFTS spectra (spectral region 1950–2250 cm^{-1}) of linearly bonded CO recorded during in adsorption–desorption equilibrium on Au/α-Fe_2O_3 at varying CO pressures between 0.5 and 10 kPa and at 80°C.

in the PROX reaction on the $Pt/\gamma\text{-}Al_2O_3$ catalyst is controlled by the high CO coverage.

3.3. CO coverage on $Au/\alpha\text{-}Fe_2O_3$

The IR vibrational spectra of the $Au/\alpha\text{-}Fe_2O_3$ catalyst during CO adsorption or oxidation are characterized by a CO band at ca. 2110 cm^{-1} (see Fig. 4), which is generally assigned to linearly adsorbed CO on single crystalline gold surfaces [26,27] and supported Au particles [28]. An asymmetric tailing on the low frequency side was interpreted by Boccuzzi et al. [19,28] in terms of a second CO adsorption state at the perimeter places on their Au/ZnO catalyst. However, since such a tailing could also emanate from a heterogeneous particle dispersion, we will refer to the band at ~ 2110 cm^{-1} as deriving from a single CO adsorption species. Additional CO species, such as CO adsorbed on (partly) ionic Au atoms (e.g., via metal–support interaction) as it had been assigned to the high frequency bands on Au/TiO_2 and Au/ZnO at 2133 cm^{-1} [19] as well as on Au/Fe_2O_3 at around 2138 and 2159 cm^{-1} [29], were not observed under our experimental conditions. The absence of these species is probably related to different catalyst pretreatment conditions and/or the presence of H_2 during our CO oxidation experiments.

Similar to the above-analysis of the CO adsorption characteristics of the $Pt/\gamma\text{-}Al_2O_3$ catalyst during the PROX reaction, we will first examine the adsorption of CO on the $Au/\alpha\text{-}Fe_2O_3$ catalyst in the absence of reaction, i.e., in a pure CO/N_2 mixture at the PROX operating temperature. DRIFTS spectra obtained at different CO partial pressures at 80°C are reproduced in Fig. 4; the resulting CO adsorption intensities and the corresponding IR frequencies are plotted in Fig. 3a and b, respectively (triangular symbols), as a function of CO partial pressure (balance N_2). Upon increasing the CO partial pressure from 0.05 to 1 kPa, the CO_{ad}-intensity increases by nearly one order of magnitude. Assuming a roughly linear relationship between signal intensity and absorber concentration, this represents a significant increase of the CO coverage on the gold particles. The conclusion is supported by a concomitant decrease in wavenumber from 2111 cm^{-1} to 2104 cm^{-1} (Fig. 3b) since υ_{CO} on gold surfaces decreases with increasing θ_{CO}, contrary to what is observed for platinum metals [30]. For comparison, the CO coverage dependence of the IR vibrational frequency of CO_{ad} on various gold surfaces reported in the literature are summarized in Table 1. In contrast to platinum, neither the adsorption temperature nor the dispersion (i.e., particle size) seem to have a significant influence on υ_{CO}. The highest values are between 2120 and 2130 cm^{-1} for the low coverage regime and generally decrease to slightly below 2110 cm^{-1}. The maximum coverage under the conditions listed in Table 1, which corresponds to the lowest wavenumbers, does not exceed $\theta_{CO} \approx 0.2$. This relatively low saturation value even at high pressures (see Table 1) may be due to a strong decrease in adsorption energy at higher adsorbate densities [26], more likely it reflects the strong variation in adsorption energy on substrate sites of different coordination, such as terrace, step or kink sites, as it had been observed recently for CO adsorption on Au single-crystals or thin films [26,27]. Therefore, a simple comparison of band positions suggests that the equilibrium CO coverage in 1 kPa CO (balance N_2) on the Au particles of our catalyst should not exceed $\theta_{CO} \approx 0.2$.

The low CO coverage under our conditions (1 kPa CO) is consistent with the data by Iizuka et al. [31], who for pure gold powder determined a coverage of ~ 0.2 at a partial pressure of 3 kPa CO and 0°C. It is furthermore consistent with an estimate based on Langmuir adsorption–desorption kinetics for CO, in conjunction with published CO adsorption energies on Au surfaces (reconstructed Au(100): 58 kJ/mol [32]; polycrystalline Au: 55 kJ/mol [33]; Au(332): 55 kJ/mol [26]; Au(110): 33 kJ/mol [34]), pre-exponential factors between 10^{13} and 10^{15} s^{-1}, and a maximum sticking coefficient of one.

In contrast to the approach used for the $Pt/\gamma\text{-}Al_2O_3$ catalyst, where the CO intensity for the pure adsorption

Table 1
CO vibrational frequency shifts as a function of CO partial pressure (and CO dosing) reported for unsupported and supported gold particles and estimated CO coverages for the maximum indicated saturation pressure

System	T [K]	Pressure range	Vibrational shift [cm^{-1}]	θ_{sat}^{a}	Reference
Au(332)	92	$2.5 \cdot 10^{-10}$–10^{-6} kPa	2124–2110	0.17	[26]
	105	$2.5 \cdot 10^{-10}$–10^{-6} kPa	2125–2113		
Au powder	273	0.7–3 kPa	–	$\sim 0.2^{b}$	[31]
Au film on Al_2O_3	2	0.01–0.8 L[c]	2125–2108		[36]
Au/SiO_2	298	0.034–10.9 kPa	2120–2110		[37]
Au/SiO_2	298	$1.7 \cdot 10^{-4}$–59 kPa	2129–2106	0.17[d]	[30]
Au/ZnO	298	2.10^{-4} kPa	2116–2106	0.22	[28]
Au/Fe_2O_3	353	0.05–1 kPa	2111–2104		this work

[a] $\theta_{sat} = \theta$ at highest pressure and lowest υ_{CO}.
[b] Calculated from their adsorption isothermes using an atomic density of 10^{19} m^{-2}.
[c] CO dosing in UHV.
[d] Coverage at 2 kPa.

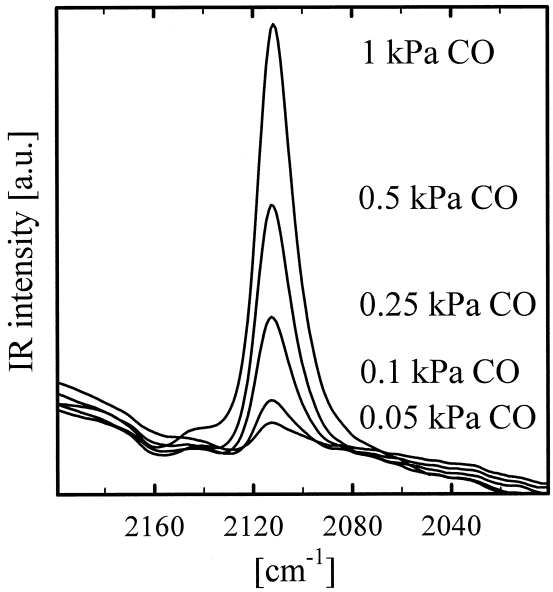

Fig. 5. In-situ DRIFTS spectra (spectral region 2000–2200 cm^{-1}) of linearly bonded CO recorded during CO oxidation in idealized reformate at $\lambda = 2$ on Au/α-Fe_2O_3 at varying CO pressures between 0.5 and 10 kPa and at 80°C.

case (CO/N_2 mixtures) was directly compared to the intensity observed under PROX conditions, this direct comparison is not possible in the case of the Au/α-Fe_2O_3 catalyst. In the latter case, the support phase changes from α-Fe_2O_3 to Fe_3O_4 in the presence of H_2 concomitant with a change in the DRIFTS signal due to a different penetration depth. Therefore, a comparison of the absolute CO intensities in CO/N_2 with those measured during selective CO oxidation in idealized reformate ($\lambda = 2$) is meaningless. We therefore estimate the steady state coverage during the PROX reaction under our experimental conditions from the adsorption/reaction kinetics. As in the case of Pt, r_{des} in Eq. (1) is several orders of magnitude larger (using the above kinetic parameters) than the TOF for the gold catalyst (see Fig. 1a), so that the CO coverage in a pure N_2 background should be the same as during the PROX reaction, i.e., ≤ 0.2 ML (assuming that the CO adsorption properties of the Au particles do not change in the presence of O_2 and H_2). To reflect the similar coverages, the CO intensities were normalized to each other at the highest CO partial pressure in Fig. 3a.

Consistent with a low CO coverage even at the highest CO partial pressure of 1 kPa (filled circles in Fig. 3a), the CO intensity/CO coverage decreases with decreasing CO partial pressure. This coverage dependence fits also to the observed positive reaction order with respect to p_{CO}, owing to a reduced reaction probability at reduced θ_{CO}.

The p_{CO}-dependence of the CO vibrational frequency during the selective CO oxidation ($\lambda = 2$) is shown in Fig. 3b (filled circles), the associated DRIFTS spectra are displayed in Fig. 5. Compared to the case of CO adsorption from a pure CO/N_2 mixture (Fig. 4), the CO frequency under PROX conditions is now shifted to significantly higher wavenumbers and barely changes with decreasing CO partial pressure (2113–2111 cm^{-1}). This increase in υ_{CO} is assigned to coadsorption of oxygen and its effect of decreasing the electron density in the gold particles. Since the bonding of CO to gold surface is dominated by the 5σ orbital [30], electron donation to the metal becomes more favorable under these conditions. Owing to the weak antibonding effect of the 5σ orbital with respect to the C–O bond, the IR band frequency would increase for a reduced electron density of the gold surface. Since Fig. 5 was recorded at a constant value of $\lambda = 2$, p_{O_2} decreases in the same way as p_{CO}, so that the up-shifting effect of O_2 is expected to be smaller. The nearly zero net shift observed in Fig. 5 (also filled symbols in Fig. 3b) can be understood as a result of these two counteracting effects (decreasing υ_{CO} with increasing θ_{CO}, but increasing wavenumber υ_{CO} with increasing p_{O_2}). A similar effect may also exist for the IR cross-section, which would explain the more pronounced decay of the intensity with smaller coverages for the PROX reaction as compared to CO adsorption.

Under the above-hypothesis of low CO coverages during the PROX reaction even at the highest CO partial pressure of 1 kPa examined in our study, it is reasonable to assume that the dissociative adsorption of hydrogen on the Au surface is not significantly perturbed by the presence of CO. Therefore, one would expect that the H_2 oxidation rate is independent of the CO partial pressure if the O_2

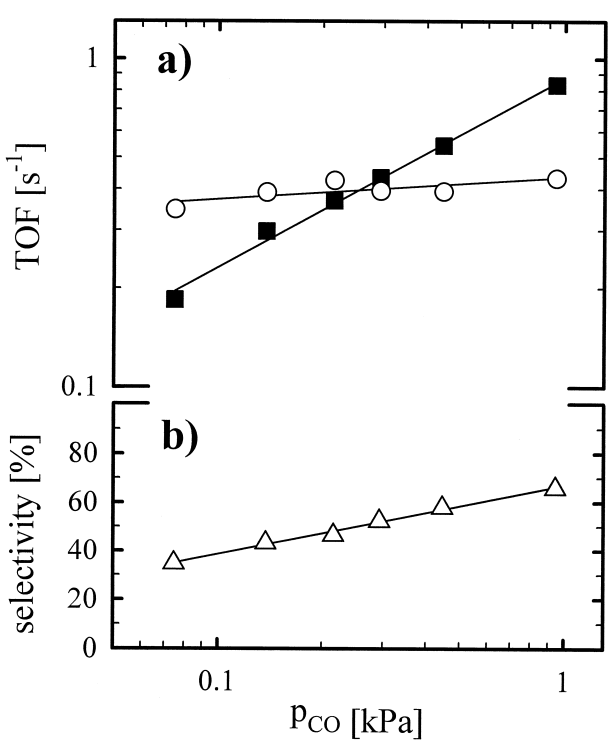

Fig. 6. (a) Rates of CO (■) and H_2 oxidation (○) and (b) selectivity (△) over Au/α-Fe_2O_3 at 80°C and $p_{O_2} = 10$ kPa in idealized reformate.

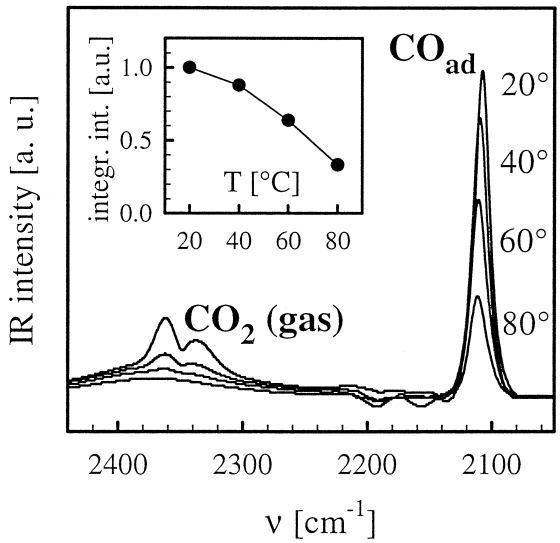

Fig. 7. In-situ DRIFTS spectra on Au/α-Fe_2O_3 during CO oxidation in idealized reformate at a constant λ of 2 at different temperatures. Inset: integrated IR intensities of linearly bound CO vs. temperature.

partial pressure remains constant. This, indeed, is confirmed by kinetic measurements on both CO and H_2 oxidation rates over Au/α-Fe_2O_3 in idealized reformate at 80°C and $p_{O_2} = 1$ kPa at 80°C, shown in Fig. 6 [9]. While the CO turnover frequency decreases with decreasing CO partial pressure owing to a decrease in CO coverage, the H_2 oxidation rate remains essentially constant (Fig. 6a). This demonstrates that r^{CO} and r^{H_2} are completely decoupled, contrary to what is observed for the Pt/γ-Al_2O_3 catalyst. As a consequence, the selectivity of the Au catalyst decreases with decreasing p_{CO} (Fig. 6b). Since the dissociative sticking probability for H_2 on a gold surface is very low [20], probably due to a strongly activated adsorption process [21], the overall selectivity is still rather high. This is different from the case of the Pt/γ-Al_2O_3 catalyst, where the high selectivity is only caused by the nearly complete blocking of the surface with adsorbed CO.

3.4. Temperature dependence

We finally present and discuss in-situ DRIFTS data recorded during the PROX reaction on Au/α-Fe_2O_3 at varying temperatures, which will provide a final piece of evidence for the hypothesis that the CO coverage under PROX conditions at 80°C is very low, far below saturation. Furthermore, these data will rationalize the observed decrease in the CO reaction during selective CO oxidation with temperature, which was found to change from +0.55 at 80°C down to +0.35 at 40°C [9]. A similar behavior was observed also by Lin et al. [35] on a 2.3 wt.% Au/TiO_2 catalyst, with a decrease in the CO reaction order from 0.6 to 0.2 as the temperature was decreased from 87° to 37°C in a H_2-free gas mixture ($p_{CO} = 1$–25 kPa, $p_{O_2} = 1$–20 kPa, balance He). Fig. 7 shows in-situ DRIFTS spectra recorded in idealized reformate (1 kPa CO, $\lambda = 2$) at 20°C, 40°C, 60°C and 80°C, respectively (all spectra taken after 30 min of equilibration). Clearly, the amount of linearly adsorbed CO decreases by a factor of three (see inset in Fig. 7) with increasing temperature. The strong decrease of the CO coverage with temperature resembles the behavior expected in the steep, middle regime of a Langmuir adsorption–desorption isobar, where the CO coverage is far below saturation, which in turn gives further credence to the hypothesis that the CO coverage under PROX conditions at 80°C is rather low on the Au/α-Fe_2O_3 catalyst. Finally, the strong variation of the steady-state CO_{ad} concentration fits well to a reaction scheme where CO supply is increasingly rate limiting, which qualitatively rationalizes the increase in CO reaction order with increasing temperature.

4. Summary

We have shown by direct in-situ DRIFTS observations that under typical reaction conditions, the reaction kinetics and the selectivity in the PROX reaction on Pt/γ-Al_2O_3 and on Au/α-Fe_2O are largely determined by the steady-state CO coverage on the active metal surfaces. Whereas in the former case, the CO coverage remains practically constant and close to saturation with varying CO partial pressure, it changes significantly with temperature or CO pressure in the latter case, with coverages below 0.2 ML at 80°C and at 1 kPa CO. The CO coverage and its variation with partial pressure and temperature not only parallel the selectivity behavior in our kinetic measurements, with practically constant selectivity on Pt/γ-Al_2O_3 and a pronounced loss in selectivity for lower CO partial pressures on Au/α-Fe_2O_3. It also rationalizes the observed CO oxidation reaction orders with respect to CO and O_2 and their temperature dependence as well as the coupling (Pt/γ-Al_2O_3) or independence (Au/α-Fe_2O_3), respectively, between H_2 and CO oxidation.

Acknowledgements

This work was supported by the Stiftung Energieforschung Baden-Württemberg (grant No. A 00008295). M.M. Schubert acknowledges a fellowship of the Deutsche Forschungsgemeinschaft via the Graduiertenkolleg: ''Molekulare Organisation und Dynamik an Grenz- und Oberflächen''. We gratefully acknowledge V. Plzak and B. Rohland (Zentrum für Sonnenenergie- und Wasserstoff-Forschung, Ulm) for the catalyst preparation and E. Auer (Degussa) for providing the platinum catalyst.

References

[1] W.S. Epling, G.B. Hoflund, J.F. Weaver, S. Tsubota, M. Haruta, J. Phys. Chem. 100 (1996) 9929.
[2] M.A. Bollinger, M.A. Vannice, Appl. Catal. B: Environmental 8 (1996) 417.
[3] A. Knell, P. Barnickel, A. Baiker, A. Wokaun, J. Catal. 137 (1992) 306.
[4] M. Haruta, S. Tsubota, T. Kobayashi, H. Kageyama, M.J. Genet, B. Delmon, J. Catal. 144 (1993) 175.
[5] M. Haruta, Catal. Surv. Jpn. 1 (1997) 61.
[6] S.K. Tanielyan, R.L. Augustine, Appl. Catal. A: General 85 (1992) 73.
[7] R.M.T. Sanchez, A. Ueda, K. Tanaka, M. Haruta, J. Catal. 168 (1996) 125.
[8] A. Grigorova, A. Palazov, J. Mellor, J.A.J. Tumilty, US Patent, 5,759,949 (issued 2/6/1998).
[9] M.J. Kahlich, H.A. Gasteiger, R.J. Behm, J. Catal. 182 (1999) 430.
[10] J.C. Trocciola, C.R. Schroll, R.R. Lesieur, US Patent, 5,330,727 (issued 19/7/1994).
[11] C. Plog, W. Maunz, T. Stengel, R. Andorf, EU Patent, 0,650,923 Al (issued 3/5/1995).
[12] S. Aoyama, EU Patent, 0,743,694 A1 (issued 20/11/1996).
[13] S. Kawatsu, J. Power Sources 71 (1998) 150.
[14] K. Eberle, B. Rohland, J. Scholta, R. Stroebel, German Patent, 19,615,562 C1 (issued 9/10/1997).
[15] M.J. Kahlich, H.A. Gasteiger, R.J. Behm, J. New Mater. Electrochem. Syst. 1 (1998) 39.
[16] M.J. Kahlich, M.M. Schubert, M. Hüttner, M. Noeske, H.A. Gasteiger, R.J. Behm, in: O. Savadogo, P.R. Roberge (Eds.), New Materials for Fuel Cells and Modern Battery Systems II, Ecole Polytechnique de Montreal, Montreal, July 06–10, 1997, p. 642.
[17] M.J. Kahlich, H.A. Gasteiger, R.J. Behm, J. Catal. 171 (1997) 93.
[18] T. Engel, G. Ertl, Adv. Catal. 28 (1979) 2.
[19] F. Boccuzzi, A. Chiorino, S. Tsubota, M. Haruta, J. Phys. Chem. 100 (1996) 3625.
[20] A.G. Sault, R.J. Madix, C.T. Campbell, Surf. Sci. 169 (1986) 347.
[21] B. Hammer, J.K. Noerskov, Nature 376 (1995) 238.
[22] K.W. van Every, P.R. Griffith, Appl. Spectrosc. 45 (1991) 347.
[23] G. Ertl, M. Neumann, K.M. Streit, Surf. Sci. 64 (1977) 393.
[24] J.S. Luo, R.G. Tobin, D.K. Lambert, G.B. Fisher, C.L. DiMaggio, Surf. Sci. 274 (1992) 53.
[25] M.R. McClellan, J.L. Gland, F.R. McFeeley, Surf. Sci. 112 (1981) 63.
[26] C. Ruggiero, P. Hollins, Chem. Soc. Faraday Trans. 92 (1996) 4829.
[27] M. Ruff, R.J. Behm, to be published.
[28] F. Boccuzzi, A. Chiorino, S. Tsubota, M. Haruta, Catal. Lett. 29 (1994) 225.
[29] S. Minico, S. Scire, A.M. Crisafulli, S. Galvagno, Catal. Lett. 47 (1997) 273.
[30] J. France, P. Hollins, J. Electron Spectrosc. Relat. Phenom. 64/65 (1993) 251.
[31] Y. Iizuka, H. Fujiki, N. Yamauchi, T. Chijiiwa, S. Arai, S. Tsubota, M. Haruta, Catal. Today 36 (1997) 115.
[32] G. McElhiney, J. Pritchard, Surf. Sci. 60 (1976) 397.
[33] M.L. Kottke, R.G. Greenler, H.G. Tompkins, Surf. Sci. 32 (1972) 231.
[34] D.A. Outka, R.J. Madix, Surf. Sci. 179 (1987) 351.
[35] S.D. Lin, M.A. Bollinger, M.A. Vannice, Catal. Lett. 17 (1993) 379.
[36] P. Dumas, R.G. Tobin, P.L. Richards, Surf. Sci. 171 (1986) 579.
[37] D.J.C. Yates, J. Colloid Interface Sci. 29 (1969) 194.